View Article Online
View Journal

Materials Horizons

Accepted Manuscript

ROYAL SOCIETY OF CHEMISTRY

rsc.li/materials-horizons

View Article Online
DOI: 10.1039/D3MH00603D

Modulating piezoelectricity and mechanical strength via three-dimensional gradient structure for piezoelectric composites

Tao Yang[1], Weili Deng [1, *], Guo Tian[1], Lin Deng[1], Wanghong Zeng[1], You Wu[1], Shenglong Wang[1], Jieling Zhang[1], Boling Lan[1], Yue Sun[1], Long Jin[1], Weiqing Yang [1,2 *]

Dr. T. Yang, Dr. G. Tian, L. Deng, W. Zeng, Y. Wu, S. Wang, J. Zhang B. Lan, Y. Sun, L. Jin,

[1] Key Laboratory of Advanced Technologies of Materials (Ministry of Education), School of Materials Science and Engineering, Southwest Jiaotong University, Chengdu 610031, P. R. China

Prof. W. Deng

[1] Key Laboratory of Advanced Technologies of Materials (Ministry of Education), School of Materials Science and Engineering, Southwest Jiaotong University, Chengdu 610031, P. R. China

E-mail: weili1812@swjtu.edu.cn

Prof. W. Yang

[1] Key Laboratory of Advanced Technologies of Materials (Ministry of Education), School of Materials Science and Engineering, Southwest Jiaotong University, Chengdu 610031, P. R. China

[2] Research Institute of Frontier Science, Southwest Jiaotong University, Chengdu 610031, PR China

E-mail: wqyang@swjtu.edu.cn

View Article Online
DOI: 10.1039/D3MH00603D

New Concepts Statement

Advanced flexible electronic devices propose an urgent demand for the wearing comfortability and the data accuracy. Piezoelectric nanocomposites composed of ceramic fillers and polymer matrices integrate complementary material properties exhibit attractive promise. However, improving the piezoelectricity of piezoelectric composites with increase the content of ceramics fillers usually lead to the sacrifice of mechanical strength. This trade-off between mechanical strength and electrical output limits the further applications. Hence, the gradient PMN-PT/PVDF nanocomposite was designed to modulate the piezoelectric property and mechanical strength. **The innovations of this work can be summarized as follows:**

1) Different gradient PMN-PT/PVDF nanocomposites was successfully constructed via the non-equilibrium process integrated with the modified electrospinning and hot-pressing process.

2) Ascribed to the unique three-dimensional gradient distribution, the prepared PMN-PT/PVDF nanocomposite exhibits excellent mechanical strength and piezoelectric performance compare to conventional nanocomposites with the randomly dispersed nanocomposite.

3) The study of gradient structure offers new opportunities to understand the structure-related mechanical and electrical behavior of nanocomposite, which is important for the design of nanocomposite.

View Article Online
DOI: 10.1039/D3MH00603D

Modulating piezoelectricity and mechanical strength via three-dimensional gradient structure for piezoelectric composites

Tao Yang[1], Weili Deng[1,] *, Guo Tian[1], Lin Deng[1], Wanghong Zeng[1], You Wu[1], Shenglong Wang[1], Jieling Zhang[1], Boling Lan[1], Yue Sun[1], Long Jin[1], Weiqing Yang [1,2] *

Dr. T. Yang, Dr. G. Tian, L. Deng, W. Zeng, Y. Wu, S. Wang, J. Zhang, B. Lan, Y. Sun, L. Jin,

[1] Key Laboratory of Advanced Technologies of Materials (Ministry of Education), School of Materials Science and Engineering, Southwest Jiaotong University, Chengdu 610031, P. R. China

Prof. W. Deng

[1] Key Laboratory of Advanced Technologies of Materials (Ministry of Education), School of Materials Science and Engineering, Southwest Jiaotong University, Chengdu 610031, P. R. China

E-mail: weili1812@swjtu.edu.cn

Prof. W. Yang

[1] Key Laboratory of Advanced Technologies of Materials (Ministry of Education), School of Materials Science and Engineering, Southwest Jiaotong University, Chengdu 610031, P. R. China

[2] Research Institute of Frontier Science, Southwest Jiaotong University, Chengdu 610031, P. R. China

E-mail: wqyang@swjtu.edu.cn

View Article Online
DOI: 10.1039/D3MH00603D

Abstract

Advanced flexible electronic devices propose an urgent demand for wearing comfort and data accuracy. Piezoelectric composites exhibit attractive promise, but mutually constrained mechanical strength and electrical output limit their further applications. Here, we design a gradient PMN-PT/PVDF nanocomposite via the non-equilibrium process integrated with the modified electrospinning and hot-pressing process to modulate piezoelectric output and mechanical strength. The enhanced piezoelectric output together with the mechanical strength of the gradient structure are verified both from the experimental and simulation results. Ascribed to the unique three-dimensional gradient distribution, the prepared PMN-PT/PVDF nanocomposite exhibits excellent mechanical strength (830 MPa) and piezoelectric performance (1.08 V), which are substantially higher than those of the randomly dispersed nanocomposite. The enhancement mechanism is revealed in terms of polarization, stress and crystallinity. These studies of gradient structure offer new opportunities to understand the structure-related mechanical and electrical behavior of nanocomposite, which supports the design of nanocomposite for overall performance.

View Article Online
DOI: 10.1039/D3MH00603D

Introduction

Dielectric materials with unique electric-coupling properties such as dielectricity, piezoelectricity, ferroelectricity and pyroelectricity have been extensively applied in electronic devices[1], energy storages[2], medical equipments[3] and military weapons[4]. Among them, the piezoelectricity of dielectric materials can convert mechanical energy into electricity, making it critical for flexible electronics[5-9] and energy harvesting[10]. Typical piezoelectric ceramics exhibit outstanding piezoelectric response, but unfortunately, the inherent brittleness and rigidness limit their applications[11-13]. In contrast, piezoelectric polymers possess weak piezoelectric response, but their good mechanical robustness and easy processing provide a worthwhile point for applications[14-16]. Thus, exploring piezoelectric materials with excellent piezoelectric performance and high mechanical strength has attracted considerable research efforts over the decades.

Nanocomposite materials integrate the complementary properties of ceramic fillers and polymer matrices, opening an effective approach to improving the comprehensive performances[17-21]. Yet, the lack of intermolecular interactions between the ceramic fillers and chemically inert polymers usually results in macroscopic phase separation of nanocomposites[22]. The mismatch of Young's modulus and spatial discontinuity between two different phases greatly hinder the force transmitting in nanocomposites, causing the degradation of piezoelectric performance[23]. Moreover, piezoceramics embedded in polymers are usually not be effectively polarized, because the large difference in dielectric constants allows the polarization field to traverse mostly across the polymer matrix[24,25], which further reduces the electrical output. To enhance the piezoelectricity of nanocomposites, a common strategy is increasing the content of piezoelectric ceramics. However, the high-volume loading of rigid ceramic fillers usually leads to poor mechanical strength[26]. In addition, the piezoelectricity of nanocomposites is not the geometric sum of the two constituents. As a result, obtaining ceramic-polymer nanocomposite materials with both excellent piezoelectric performance and mechanical strength is still a great challenge.

The arrangement of ceramic filler in nanocomposite materials determines the

electromechanical coupling, which significantly influences the piezoelectric performance. According to the self-connected state of ceramic fillers, either one, two or three dimensions, ten connectivity patterns for the two-phase system have been developed, in which the composite types of 0-3, 1-3 and 2-2 achieved the best piezoelectricity[27]. Unfortunately, the trade-off between mechanical toughness and piezoelectric performance still exists at these nanocomposites. Recently, the emerging gradient structure has exhibited exciting modulation capabilities by optimizing the connectivity pattern of fillers, offering a potential opportunity to improve the comprehensive performance of the nanocomposite materials[28-31]. For instance, the highly oriented barium titanite significantly enhances the dielectric constant of $BaTiO_3$/epoxy with lamellar composite architectures[32]. The graded heterostructure of PZT film exhibits excellent piezoelectric performance[33]. The barium zirconate titanate and hexagonal boron nitride with an interpenetrating gradient structure demonstrate ultrahigh discharge energy density[34]. In this work, the PMN-PT/PVDF nanocomposites with gradient concentration distribution along the out-of-plane direction were constructed to optimize the piezoelectricity, dielectricity and mechanical strength at the same time. The mechanical strength and electrical output of the PMN-PT/PVDF nanocomposites were systematically characterized, respectively. In addition, the corresponding mechanism was revealed with finite element analysis (FEA) simulation. These studies provide an effective strategy for achieving piezoelectric nanocomposites simultaneously with high mechanical strength and excellent piezoelectric performance.

Results and Discussion

Microstructure of gradient PMN-PT/PVDF nanocomposites

To further enhance the piezoelectricity and mechanical strength of piezoelectric composites, the gradient nanocomposites of small-large-small concentration components (G_{030}-PMN-PT) and large-small-large concentration components (G_{303}-PMN-PT) were prepared along the out-of-plane direction of the film, separately. For the gradient structure of G_{030}-PMN-PT, the concentration of PMN-PT particles increases linearly from the outer surface (0 vt%) to the center (30 vt%) and the particles

are seldom in the surface layer of the film, as shown in **Figures 1a** and **b-ⅱ**. Another gradient structure of G_{303}-PMN-PT is organized via the reverse structure of PMN-PT particle concentration, so the particles are abundant in the surface layer of the film, as illustrated in **Figures 1a** and **b-ⅲ**. In contrast, the conventional composite is constructed with PMN-PT particle fillers (15 vt%) randomly dispersed in the PVDF matrix (R-PMN-PT), where the particles are moderate in the whole matrix (**Figures 1a** and **b-ⅰ**).

From the optical graph presented in **Figure 1c**, the homogeneous dispersion of PMN-PT particles demonstrates the uniformity of the films. And the high-quality freestanding film with a smooth surface and curved shape displays promising potential for flexible electronics (**Figure 1d**). According to previous studies, the stress concentration caused by the gradient structure facilitates the piezoelectric outputs. The crystallization regions in polymer matrix of the composites contribute to mechanical strength. Thus, the piezoelectric composites with gradient structure of G_{303}-PMN-PT are expected to exhibit higher piezoelectricity and mechanical strength than G_{030}-PMN-PT and randomly dispersed structures. In addition, the unique trend of dielectric constant and impedance are also observed in the composite materials. **Figure 1e** summarizes the possible relationships between the gradient structure and randomly dispersed structure for several performance metrics, including piezoelectric coefficients d_{33}, dielectric constant, piezoelectric output voltage, tensile modulus and impedance Zp'.

View Article Online
DOI: 10.1039/D3MH00603D

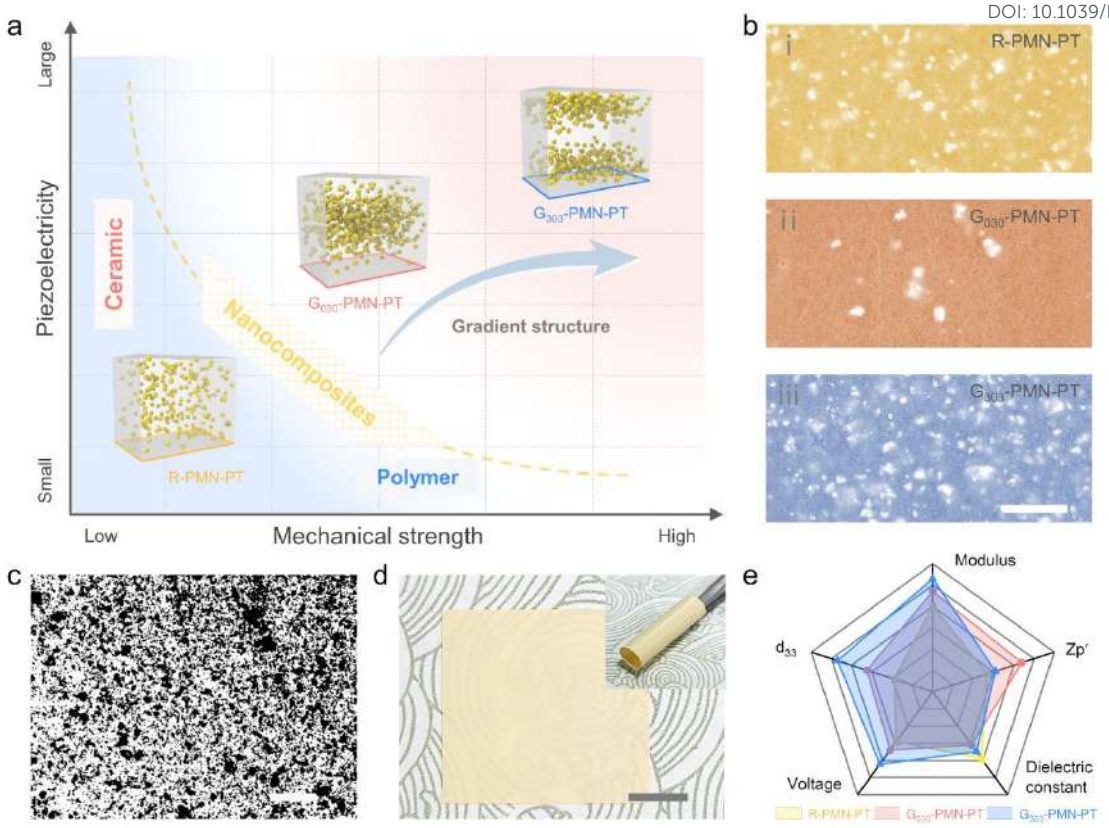

Figure 1. Microstructure of gradient PMN-PT/PVDF nanocomposites. a) Abstract model of nanocomposites with gradient structure to enhance piezoelectricity and mechanical strength. b) SEM images of the PMN-PT/PVDF nanocomposite films surface with nanoparticles randomly and gradient dispersed in the matrix. Scale bars, 5 μm. c) Optical microscope image of PMN-PT/PVDF nanocomposites with light transmission through the sample. Scale bar, 50 μm. d) Photograph of the gradient structure film with high uniformity and flexibility. Scale bar, 5 mm. e) Performance comparison of films with gradient structure and random structure in terms of piezoelectric coefficient d_{33}, dielectric constant, piezoelectric output voltage, tensile modulus and impedance Zp'.

Preparation of gradient PMN-PT/PVDF nanocomposites

The gradient PMN-PT/PVDF nanocomposites were fabricated through a non-equilibrium process that integrated a modified electrospinning and hot-pressing process. Notably, two vertical-aligned syringes with programmable flow rates are employed to fabricate the gradient structure (**Figure 2a**). Taking the gradient G_{030}-PMN-PT as an

example, when the content of PMN-PT increases linearly from the surface to the center of the film, the flow rate of pure PVDF precursor solution first decreases then increases and vice versa for the PMN-PT/PVDF precursor solution. After collecting the stacked multilayer nanofibers with gradient concentration, the integrity film with gradient structure was hot-pressed near the melting temperature. Alternatively, the structure of gradient G_{303}-PMN-PT and R-PMN-PT film can be obtained via the same procedure. As shown in **Figure 2b**, the PMN-PT nanoparticles embedded in the PVDF matrix facilitate the electric-coupling and mechanical transmission. And the corresponding Energy-dispersive X-ray spectroscopy (EDS) pattern of the nanocomposite further verifies the well-match distribution of the nanoparticles (Pb elements) and the polymer matrix (C and F elements) in **Figure 2c**. Compared to the Raman intensity mapping of electroactive β-phase (**Figure 2d**), the nanoparticles are well encapsulated with the electroactive phase, which contributes to the piezoelectric performance.

To investigate the microstructure properties of the gradient nanocomposite materials, X-ray diffraction (XRD), Fourier transform infrared (FTIR) and Raman spectra have been characterized. From XRD patterns (**Figure 2e**), PMN-PT/PVDF nanocomposite films are clearly identified with the typical diffraction peak of 20.8° corresponding to the β-phase of PVDF and the classical diffraction peaks of 31.4° and 44.7° matched with polycrystalline perovskite phase of PMN-PT. The β-phase of PVDF and the perovskite phase for PMN-PT nanoparticles present the most favorable piezoelectricity, which would synergistically increase the piezoelectric performance of nanocomposites. Through the FTIR spectroscopy in **Figure 2f**, the apparent absorption peak at 840 cm^{-1} confirms the almost pure β-phase after the non-equilibrium processes for the PVDF matrix, and the weak absorption peak at 765 cm^{-1} suggests the minimal content of non-polarized α-phase. The high content of β-phase in composite is mainly attributed to two aspects: the in-situ electric poling and stretching force exerted on the fibers during the electrospinning[16] and the abundant interfacial stress during the hot-pressing process of the nanofibers film[35]. The obvious peak at 838 cm^{-1} in Raman spectra further confirms the β-phase in composites after the non-equilibrium manufacturing process, as shown in **Figure 2g**.

View Article Online
DOI: 10.1039/D3MH00603D

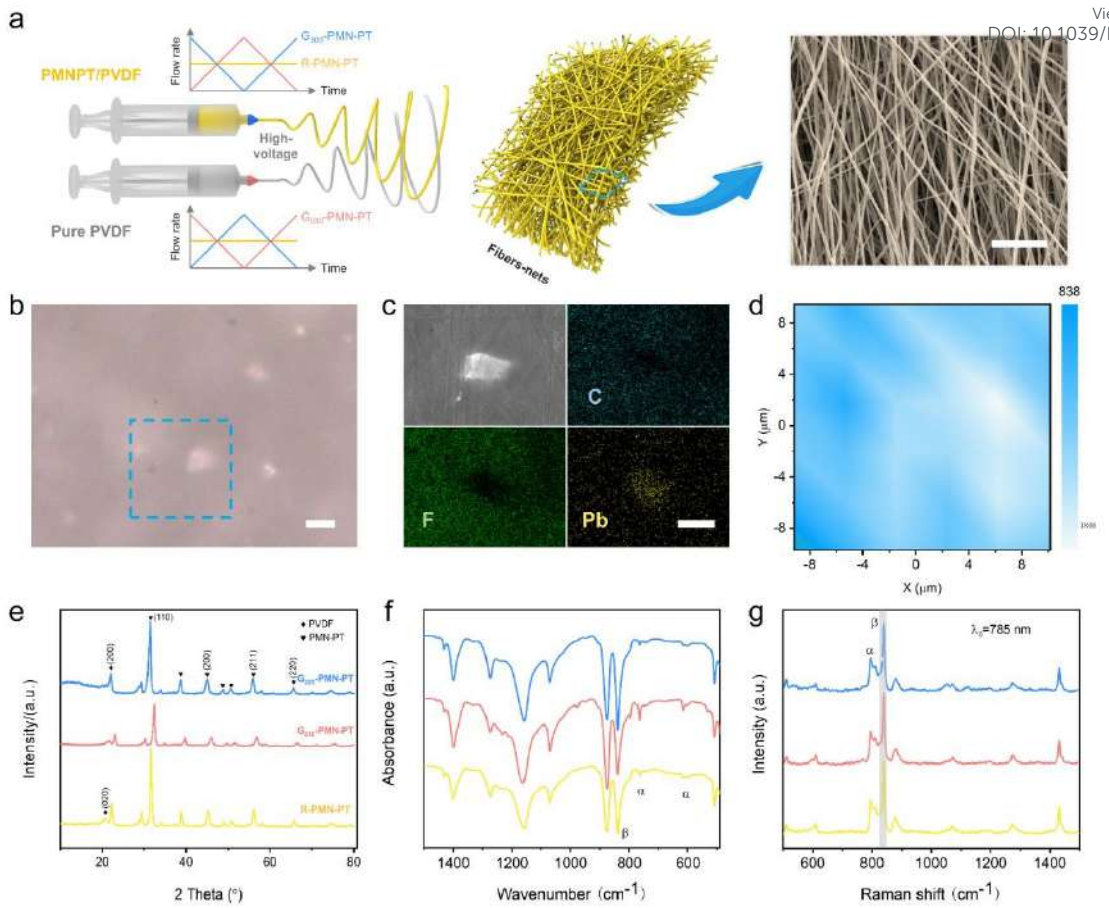

Figure 2. Preparation of gradient PMN-PT/PVDF nanocomposites. A) Schematic illustration of the modified electrospinning process for gradient nanofibers film. Scale bar of the SEM image is 5 μm. B) Optical image of the film surface, with the blue square area used for Raman mapping measurement. Scale bar, 5 μm. C) EDS mapping of C, F and Pb for PMN-PT nanoparticles embedded in PVDF matrix. Scale bar, 2 μm. D) Two-dimensional Raman mapping of the nanoparticles embeds in polymer matrix with the β-phase intensities (838 cm^{-1}). Blue corresponds to the β-phase and the white indicates the PMN-PT nanoparticles. E-g) XRD, FTIR and Raman spectra of the G_{303}-PMN-PT, G_{030}-PMN-PT and R-PMN-PT films.

Mechanical strength of gradient PMN-PT/PVDF nanocomposites

The flexible electronics and energy harvesting device requires not only the piezoelectric performance of the composite materials, but also the mechanical robustness and toughness, which determine user comfort and device durability. Hence, the mechanical strength of gradient structure materials was measured by uniaxial

stretching experiments at room temperature[36]. In which, the strain fractures, tensile strength and tensile modulus were analyzed. First, all the prefabricated films were cut into a rectangle for stretching, as illustrated in the inset of **Figure 3a**. Comparing the tensile stress-strain curves measured at a steady rate of 5 mm/s, all the films exhibit a consistent evolutionary trend with a linear increase within a slight strain, followed by a non-linear increase until the final fracture. The G_{303}-PMN-PT presents a maximum strain fracture of 22% and tensile strength of 55 Mpa, while the R-PMN-PT are 10% and 39 Mpa, respectively. And the highest tensile modulus of G_{303}-PMN-PT is 830 Mpa in contrast to the R-PMN-PT is 706 Mpa, as shown in **Figure 3b**. Obviously, the strain fractures and tensile strengths of the gradient structure are both greater than those of the random structure, demonstrating a reinforced mechanical strength of the gradient film.

In order to explain the high mechanical strength of the gradient structure, the crystalline structure in polymer matrix was characterized with differential scanning calorimetry (DSC). Accordingly, the large melting enthalpy of 60.4 J/g, 55.4 J/g and 42.4 J/g for G_{303}-PMN-PT, G_{030}-PMN-PT and R-PMN-PT, respectively, could be extracted from the DSC spectra (**Figure 3c**). The melting enthalpy of polymers is proportional to the crystallinity. The crystallinity can be calculated by the equation $\Delta X_c = \Delta H / \Delta H_m$, where ΔH is the melting enthalpy obtained by integrating the melting peak of composites, ΔH_m is the melting enthalpy of PVDF with 100% crystallinity (104.5 J g^{-1})[37]. The crystallinities of the G_{303}-PMN-PT and G_{030}-PMN-PT are 57.8% and 53%, which are greater than 40.5% of R-PMN-PT. Incorporation with the cross-sectional SEM images in **Figure 3d**, these results can be revealed with the full crystallization for gradient structure in polymer-dominant layer and the confined crystallization for the randomly dispersed structure within the three-dimensional network of the polymer matrix. To better understand this mechanism, the abstract models of the crystal regions distribution are constructed in **Figure 3d.** The larger continuous crystalline regions are observed in the gradient structure, revealing the outstanding mechanical performance of G_{303}-PMN-PT structure films.

View Article Online
DOI: 10.1039/D3MH00603D

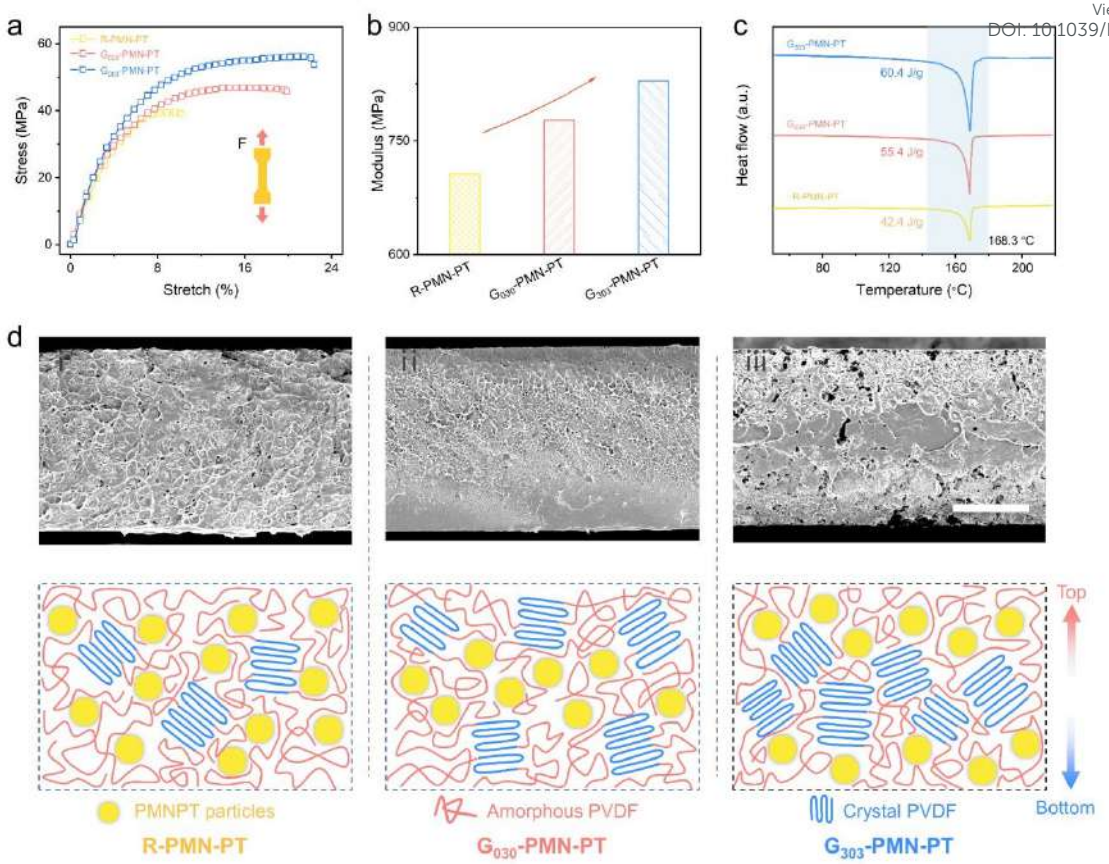

Figure 3. Mechanical strength of gradient PMN-PT/PVDF nanocomposites. A) Stress-strain curves of gradient structure films with tensile testing at a constant speed of 5 mm/s. b) Tensile modulus of gradient structure films obtained from stress-strain curves. C) DSC spectra of the gradient structure films. D) Cross-sectional SEM images and corresponding abstract models of crystal region for gradient structure films.

Piezoelectric performance of gradient PMN-PT/PVDF nanocomposites

The polarization of dielectric materials is closely related to the piezoelectric performance, which can be investigated by ferroelectric and dielectric measurements. To explore the polarization under electric field, the conformally smoothed Ag electrodes were coated on both sides of gradient composite films by magnetron sputtering. Then the unipolar polarization responses of the composite films were recorded with electrical polarization-electric field (P-E) loops and plotted in **Figure 4a** and **Figure S1**. The remnant polarization (P_r) and maximum polarization (P_{max}) of G_{303}-PMN-PT and G_{030}-PMN-PT are slightly lower than that of R-PMN-PT due to the low polarization electric field across the polymer-rich layer. Furthermore, different abstract

distribution models of nanoparticles were constructed to explore the electric polarization response via FEA simulation. For the R-PMN-PT structure, the interactions of randomly dispersed nanoparticles induce higher polarization in the polymer matrix[4], while the weaker interactions among the densely stacked nanoparticles of G_{303}-PMN-PT and G_{030}-PMN-PT reduce polarization in the polymer matrix. These FEA simulation results are well in agreement with the measured P_r and P_{max} of the gradient composite films. Similarly, the same evolutionary trend is observed from the dielectric constant measurement, as displayed in **Figure 4b** and **Figure S2**. Benefiting from the gradient structure, the low dielectric loss is achieved because the polymer layer hinders the electron transfer[37]. In addition, piezoelectric strain is well linearly related to the electric field below the coercivity field of ferroelectric materials. From the strain-electric field (S-E) curves in **Figure 4c**, the remarkably larger strain of the gradient structure suggests a higher piezoelectric response. Moreover, the obvious 180° phase reversal confirms the strain stems from the inverse piezoelectric effect, as shown in **Figure S2c**. The calculated piezoelectric coefficient of G_{303}-PMN-PT is 15.5 pm/V, while 9.9 pm/V for R-PMN-PT.

The schematic diagram of a piezoelectric material generating electric charges in response to mechanical force is illustrated in the upper part of **Figure 4d**. For piezoelectric composites, the mismatch of Young's modulus between the nanoparticles and polymer usually leads to stress concentration, which facilitates piezoelectric output[38]. The FEA simulation results show that the inhomogeneous distribution of nanoparticles makes a significant stress concentration in the gradient structure, as displayed in the lower part of **Figure 4d**. Especially, the maximum stress of G_{303}-PMN-PT is larger than that of G_{030}-PMN-PT due to its higher Young's modulus of the composites. According to our previous research on piezoelectric device models[39], the piezoelectric output positively relates to the device resistance. The gradient structure endows the higher impedance at the cost of the dielectric constant (**Figure 4e**), which helps to increase the piezoelectric output. To further verify the piezoelectric output on the direct piezoelectric effect, the gradient structure device was periodically loaded with

the linear motor at a frequency of 1 Hz (**Figure S3**). As presented in **Figure 4f and Figure S4**, the multicycle response curves of voltage and charge indicate the stable performance of the devices. With the pressure increased from 4 N to 24 N, the output voltage and charge monotonically increase for all the samples (**Figure 4g**). The gradient structure exhibits higher piezoelectric output than R-PMN-PT, with G_{303}-PMN-PT showing the best output, which can be attributed to larger stress concentration and impedance. To further verify the piezoelectric performance, the piezoelectric voltage outputs were explored via the FEA simulation (**Figure S5**). The simulation results are highly in agreement with the experimental results, which further demonstrate the increase of piezoelectric output (**Figure 4h**). The proposed gradient structure design provides an effective strategy to modulate the piezoelectricity and mechanical strength of piezoelectric nanocomposites in contrast to other piezoelectric materials[22, 23, 40-43] (**Table 1**).

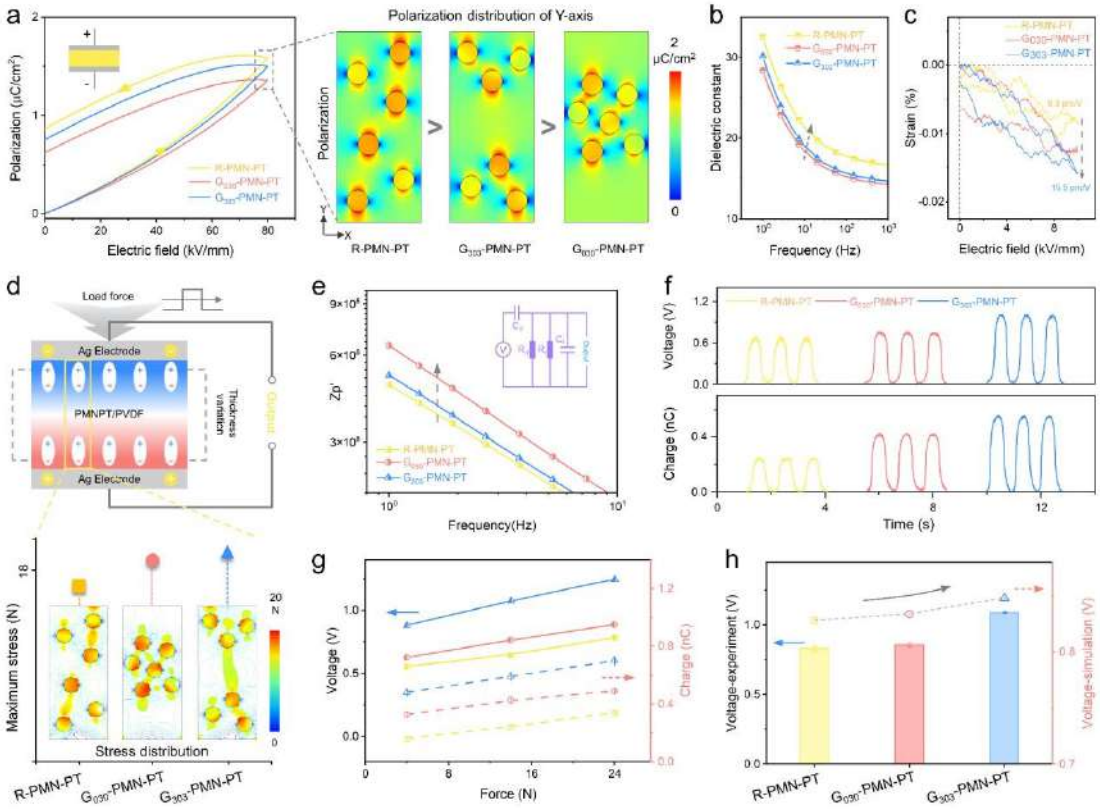

Figure 4. Piezoelectric performance of gradient PMN-PT/PVDF nanocomposites. a) Polarization of the gradient structure measured with polarization-electric (P-E) field hysteresis loops and the local electric field distribution in FEA results. b) Frequency-

dependent dielectric constant of the gradient structure films with frequency from 1 to 10^3 Hz. c) Strain-electric field (S-E) curves under AC electric field of 1 Hz. d) Schematic of the direct piezoelectric effect and stress concentrations in FEA results. e) Impedance of gradient structure films with frequency from 1 to 10 Hz and the diagram of the testing circuit. f) Charge and output voltage of the piezoelectric device under the same pressures at the same frequency. g) Charge and output voltage of the piezoelectric device increase with force. h) Comparison of output voltages under experimental tests and simulations.

Conclusions

In conclusion, the three-dimensional gradient PMN-PT/PVDF film was successfully prepared through a modified electrospinning and hot-pressing process. Compared with the randomly dispersed nanocomposites, the high crystallinity of the gradient structure greatly improved the mechanical robustness with the largest tensile strength of 55 MPa and tensile modulus of 830 MPa in G_{303}-PMN-PT. Based on the non-homogenous distribution of PMN-PT nanoparticles, the higher impedance and the stress concentration were induced to enhance piezoelectricity. The maximum piezoelectric output voltage is 1.08 V, with a piezoelectric coefficient of 15.5 pm/V for G_{303}-PMN-PT. The advanced gradient structure reinforces the mechanical strength and piezoelectric output simultaneously, supporting the expansion of piezoelectric composites for wearable electronics and energy harvesting applications.

Experimental methods

Fabrication of PMN-PT nanoparticles

The PMN-PT [$(Pb(Mg_{1/3}Nb_{2/3})O_3)_{0.7}$-$(PbTiO_3)_{0.3}$] powers with pure perovskite phase were purchased from Kaistar Electro-optic Materials Co. Ltd. Then, the PMN-PT particles were prepared according to the process, as shown in **Figure S6**. First, the polyvinyl alcohol (PVA 15 wt%) binder was mixed with the powder through milling and dried with an infrared lamp. Then the mixed powers were pressed into pellets with diameters of 1 cm and thickness of 0.5 mm under pressing of 10 MPa for 5 min. To

remove the binder, the pellets were sintered at 600 ℃ of 1 h with a heating rate of 1 ℃/min and the temperature was then increased to 1100 ℃ for 3 h to obtain high densities. The sliver paste was coated on both sides of pellets and sintered at 600 ℃ for 15 min. These pellets with silver electrodes were poled in silicone oil at 120 ℃ for 15 min under a voltage of 1.2 kV to induce high piezoelectricity. After 10 h of high-energy milling, the PMN-PT power with high piezoelectricity was obtained.

Fabrication of gradient films

The gradient structure was constructed with the non-equilibrium process, which combined the modified electrospinning and hot-pressing process. PVDF (Mw~180000) was obtained from Sigma Aldrich. The precursor solution of PVDF was prepared by dissolving PVDF (25 wt%) into a mixture solution (7:13 v/v) of acetone and dimethylacetamide (DMAc) with magnetic stirring at 60 ℃ for 2 h. In addition, the PMN-PT/PVDF precursor solution was obtained by further adding PMN-PT (30 vt%) nanoparticles to PVDF solution with ultrasonication and magnetic stirring. Then the obtained precursor solution was transferred into two syringes equipped with programmable pumps, respectively. And the electrospinning was carried out under a voltage of 17 kV and collected with a roller at a distance of 12 cm. The gradient fibrous mats were produced by regulating the flow rates of these two precursor solutions. The fibrous mats were pressed to uniform films by hot-pressing at 165 ℃ for 30 min followed by quenching water. The randomly dispersed film was prepared with a non-equilibrium process for comparison with the same volume fraction of PMN-PT (15 vt%).

Structure characterizations

The characterizations of the gradient composites and nanofibers morphology were performed with scanning electron microscopy (SEM, JSM 7800F) and energy disperse spectroscopy (EDS). The crystal structure of PMN-PT and PVDF were characterized with X-ray diffraction (XRD, HomeLAB) with Cu Kα radiation (λ=0.15405 nm). The chain conformations of the polymer matrix were analyzed by Fourier transform infrared (FTIR, Nicolet iS50), Raman (Lab RAM HREvolution) and differential scanning calorimetry (DSC 2500). The Raman mapping was carried out under 785 nm excitation

to verify the distribution of PMN-PT nanoparticles. The mechanical strength of the gradient composite was detected by the tensile testing system (JHY-5000).

Fabrication of the flexible pressure sensor

Firstly, the racket-shaped Ag electrode was deposited on both sides of the films through the radio frequency magnetron sputtering. The Ag target was purchased from the ZhongNuo Advanced Material (Beijing) Technology Co., Ltd. Then the conductive carbon tapes were attached on the electrode to transfer the piezoelectric output. Finally, the device was sealed with polyurethane (PU) to avoid the disturbance of external environment.

Piezoelectric and Dielectric Performance Measurement

Dielectric constant and loss factor were recorded using the Alpha-A High Performance Frequency Analyzer with frequencies ranging from 1 Hz to 10 MHz at a bias of 1 V. The electric-induced polarization and piezoelectric coefficients were determined by a ferroelectric test system (TF Analyzer 2000E, aixACCT, TREK 610E,) at a frequency of 1 Hz at room temperature. The piezoelectric output voltage and charge under dynamic forces were acquired with a linear motor (LinMot H01-23×86/160) equipped with a force gauge (IMADA model ZPS-DPU-50N) and Keithley 6514. The dynamic pressure was controlled by adjusting the distance between the compressing plate and the sample surface. The simulated piezoelectric output and stress distribution were studied with finite element analysis (FEA) software COMSOL Multiphysics.

Data availability

All data need to evaluate the conclusion in the paper are present in the paper or the supporting information. Additional data can be obtained from the authors upon reasonable request.

Author contributions

Tao Yang: investigation, conceptualization, formal analysis, writing-original draft. Weili Deng: conceptualization, supervision, funding acquisition, editing & revision. Guo Tian: methodology, investigation. Lin Deng: methodology, investigation. Wanghong Zeng: methodology. You Wu: methodology, data analysis. Shenglong

Wang: Software. Jieling Zhang: data analysis. Boling Lan: software. Yue Sun: data analysis. Long Jin: supervision. Weiqing Yang: conceptualization, funding acquisition, editing & revision.

Competing interests

The authors declare no competing interests.

Acknowledgements

This research was financially supported by Sichuan Science and Technology Program (No. 2023NSFSC0313) and the Sichuan Province Foundation for Distinguished Young Team (No. 20CXTD0106). Thanks for the help from the Analysis and Testing Center of Southwest Jiaotong University.

Additional information

The online version contains supplementary material available at

References

1. H. C. Ates, P. Q. Nguyen, L. Gonzalez-Macia, E. Morales-Narváez, F. Güder, J. J. Collins and C. Dincer, *Nat. Rev. Mater.*, 2022, **7**, 887-907.
2. Q.-K. Feng, S.-L. Zhong, J.-Y. Pei, Y. Zhao, D.-L. Zhang, D.-F. Liu, Y.-X. Zhang and Z.-M. Dang, *Chem. Rev.*, 2022, **122**, 3820-3878.
3. H. Hu, H. Huang, M. Li, X. Gao, L. Yin, R. Qi, R. S. Wu, X. Chen, Y. Ma, K. Shi, C. Li, T. M. Maus, B. Huang, C. Lu, M. Lin, S. Zhou, Z. Lou, Y. Gu, Y. Chen, Y. Lei, X. Wang, R. Wang, W. Yue, X. Yang, Y. Bian, J. Mu, G. Park, S. Xiang, S. Cai, P. W. Corey, J. Wang and S. Xu, *Nature*, 2023, **613**, 667-675.
4. X. Huang, B. Sun, Y. Zhu, S. Li and P. Jiang, *Prog. Mater. Sci.*, 2019, **100**, 187-225.
5. W. Deng, Y. Zhou, A. Libanori, G. Chen, W. Yang and J. Chen, *Chem. Soc. Rev.*, 2022, **51**,3380-3435.
6. C. Zhao, X. Zhang, G. Chen and L. Shang, *Mater. Futures*, 2022, **1**, 022401.
7. T. H. Wong, C. K. Yiu, J. Zhou, Z. Song, Y. Liu, L. Zhao, K. Yao, W. Park, W. Yoo, E. Song, Z. Xie, X. Yu, *Soft Sci.*, 2021, **1**, 10.
8. J. Liu, G. Tian, W. Yang and W. Deng, *Soft Sci.*, 2022, **2**, 22.
9. J. Zhu, C. Zhou and M. Zhang, *Soft Sci.*, 2021, **1**, 3.
10. N. A. Shepelin, A. M. Glushenkov, V. C. Lussini, P. J. Fox, G. W. Dicinoski, J. G. Shapter and A. V. Ellis, *Energy Environ. Sci.,* 2019, **12**, 1143-1176.
11. Y. Liu and Y. Wang, *J. Chin. Ceram. Soc.*, 2022, **50**, 625-641.
12. Y. Yang, T. Cui, D. Li, S. Ji, Z. Chen, W. Shao, H. Liu, T-L. Ren, *Nano-Micro Lett.*, 2022, **14**, 161.
13. Y. Sun, S. Shen, W. Deng, G. Tian, D. Xiong, H. Zhang, T. Yang, S. Wang, J. Chen and W. Yang, *Nano Energy*, 2023, **105**, 108024.
14. D. Yu, Z. Zheng, J. Liu, H. Xiao, G. Huangfu, Y. Guo, *Nano-Micro Lett.*, 2021, **13**, 117.
15. X. Chen, H. Qin, X. Qian, W. Zhu, B. Li, B. Zhang, W. Lu, R. Li, S. Zhang, L. Zhu, F. D. D.

View Article Online
DOI: 10.1039/D3MH00603D

Santos, J. Bernholc, Q. M. Zhang, *Science*, 2022, **375**, 1418-1422.
16. B. Lan, X. Xiao, A. D. Carlo, W. Deng, T. Yang, L. Jin, G. Tian, Y. Ao, W. Yang and J. Chen, *Adv. Funct. Mater.*, 2022, **32**. 2207393.
17. B. Stadlober, M. Zirkl and M. Irimia-Vladu, *Chem. Soc. Rev.*, 2019, **48**, 1787-1825.
18. L. Lu, W. Ding, J. Liu and B. Yang, *Nano Energy*, 2020, **78**, 105251.
19. Q. Li, L. Chen, M. R. Gadinski, S. Zhang, G. Zhang, U. Li, E. Iagodkine, A. Haque, L. Q. Chen, N. Jackson and Q. Wang, *Nature*, 2015, **523**, 576-579.
20. Z.-H. Shen, Z.-W. Bao, X.-X. Cheng, B.-W. Li, H.-X. Liu, Y. Shen, L.-Q. Chen, X.-G. Li and C.-W. Nan, *NPJ Comput. Mater.*, 2021, **7**, 110.
21. L. Deng, W. Deng, T. Yang, G. Tian, L. Jin, H. Zhang, B. Lan, S. Wang, Y. Ao, B. Wu and W. Yang, *J. Funct. Biomater.*, 2023, **14**, 37.
22. Y. Hong, B. Wang, Z. Long, Z. Zhang, Q. Pan, S. Liu, X. Luo and Z. Yang, *Adv. Funct. Mater.*, 2021, **31**, 2104737.
23. Q. Li, L. Chen, M. Guo and Z. Hu, *Adv. Mater. Technol.*, 2022, **7**, 2101371.
24. G. Tian, W. Deng, T. Yang, D. Xiong, H. Zhang, B. Lan, L. Deng, B. Zhang, L. Jin and H. Huang, Y. Sun, S. Wang and W. Yang. *Small*, 2207947.
25. L. Li, J. Cheng, Y. Cheng, T. Han, Y. Liu, Y. Zhou, G. Zhao, Y. Zhao, C. Xiong, L. Dong and Q. Wang, *Adv. Mater.*, 2021, **33**, 2102392.
26. X. Chen, T. Yang, Q. Zhang, L. Q. Chen, V. Bobnar, C. Rahn and Q. M. Zhang, *Nano Energy*, 2021, **88**, 106225.
27. F. Narita and M. Fox, *Adv. Eng. Mater.*, 2018, **20**, 1700743.
28. S. Wang, W. Deng, T. Yang, Y. Ao, H. Zhang, G. Tian, L. Deng, H. Huang, J. Huang, B. Lan and W. Yang, *Adv. Funct. Mater.* 2023, 2214503.
29. D. Xiong, W. Deng, G. Tian, B. Zhang, S. Zhong, Y. Xie, T. Yang, H. Zhao and W. Yang, *Nano Energy*, 2022, **93**, 106889.
30. H. Liu, X. Lin, S. Zhang, Y. Huan, S. Huang and X. Cheng, *J. Mater. Chem. A*, 2020, **8**, 19631-19640.
31. B. Lan, T. Yang, G. Tian, Y. Ao, L. Jin, D. Xiong, S. Wang, H. Zhang, L. Deng, Y. Sun, J. Zhang W. Deng and W. Yang, *ACS Appl. Mater. Interfaces*, 2023, **15**, 12146-12153.
32. R. Guo, J. I. Roscow, C. R. Bowen, H. Luo, Y. Huang, Y. Ma, K. Zhou and D. Zhang, *J. Mater. Chem. A*, 2020, **8**, 3135-3144.
33. D. Zou, S. Liu, C. Zhang, Y. Hong, G. Zhang and Z. Yang, *Nano Energy*, 2021, **85**, 105984.
34. J. Jiang, Z. Shen, X. Cai, J. Qian, Z. Dan, Y. Lin, B. Liu, C. W. Nan, L. Chen and Y. Shen, *Adv. Energy Mater.*, 2019, **9**, 1803411.
35. N. Meng, X. Ren, G. Santagiuliana, L. Ventura, H. Zhang, J. Wu, H. Yan, M. J. Reece and E. Bilotti, *Nat. Commun.*, 2019, **10**, 4535.
36. X. Zhang, J. Jiang, Z. Shen, Z. Dan, M. Li, Y. Lin, C. W. Nan, L. Chen and Y. Shen, *Adv. Mater.*, 2018, **30**, e1707269.
37. X. Qian, D. Han, L. Zheng, J. Chen, M. Tyagi, Q. Li, F. Du, S. Zheng, X. Huang, S. Zhang, J. Shi, H. Huang, X. Shi, J. Chen, H. Qin, J. Bernholc, X. Chen, L. Q. Chen, L. Hong and Q. M. Zhang, *Nature*, 2021, **600**, 664-669.
38. M. Yuan, R. Ma, Q. Ye, X. Bai, H. Li, F. Yan, C. Liu, Y. Ren and Z. Wang, *Chem. Eng. J.*, 2023, **455**, 140771.
39. G. Tian, W. Deng, D. Xiong, T. Yang, B. Zhang, X. Ren, B. Lan, S. Zhong, L. Jin, H. Zhang,

View Article Online
DOI: 10.1039/D3MH00603D

L. Deng and W. Yang, *Cell Rep. Phys. Sci.*, 2022, **3**, 100814.

40. T. Kowalchik, F. Khan, K. Le, P. Leland, S. Roundy and R. Warren, *Nano Energy*, 2023, **109**, 108276.
41. F. Yang, J. Li, Y. Long, Z. Zhang, L. Wang, J. Sui, Y. Dong, Y. Wang, R. Taylor, D. Ni, W. Cai, P. Wang, T. Hacker and X. Wang, Science, 2021, 373, 337-342.
42. T. Tang, Z. Shen, J. Wang, S. Xu, J. Jiang, J. Chang, M. Guo, Y. Fan, Y. Xiao, Z. Dong, H. Huang, X. Li, Y. Zhang, D. Wang, L-Q. Chen, K. Wang, S. Zhang, C-W. Nan and Y. Shen, Natl. Sci. Rev., *2023*, nwas177.
43. J. Li, F. Yang, Y. Long, Y. Dong, Y. Wang and X. Wang, *ACS Nano*, 2021, **15**, 14903-14914.